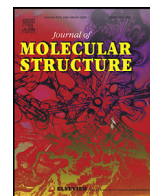




Since January 2020 Elsevier has created a COVID-19 resource centre with free information in English and Mandarin on the novel coronavirus COVID-19. The COVID-19 resource centre is hosted on Elsevier Connect, the company's public news and information website.

Elsevier hereby grants permission to make all its COVID-19-related research that is available on the COVID-19 resource centre - including this research content - immediately available in PubMed Central and other publicly funded repositories, such as the WHO COVID database with rights for unrestricted research re-use and analyses in any form or by any means with acknowledgement of the original source. These permissions are granted for free by Elsevier for as long as the COVID-19 resource centre remains active.



Evaluating anti-coronavirus activity of some phosphoramides and their influencing inhibitory factors using molecular docking, DFT, QSAR, and NCI-RDG studies

Khodayar Gholivand^{1,*}, Fahimeh Mohammadpanah¹, Mahsa Pooyan¹,
Roohollah Roohzadeh¹

Department of Chemistry, Faculty of Science, Tarbiat Modares University, Tehran, Iran

ARTICLE INFO

Article history:

Received 2 June 2021

Revised 8 September 2021

Accepted 9 September 2021

Available online 12 September 2021

Keywords:

COVID-19 main protease (M^{pro})

Phosphoguanidine

Phosphopyrazine

Docking

QSAR

ABSTRACT

The recent prevalence of coronavirus disease in 2019 (COVID-19) has triggered widespread global health concerns. Antiviral drugs based on phosphoramides have significant inhibitory activity against the main protease (M^{pro}) of the virus and prevent transcription and viral replication. Hence, in order to design and introduce a group of inhibitors affecting the coronavirus, 35 phosphoramide compounds based on phospho-guanine and phospho-pyrazine derivatives were selected for molecular docking study. The results showed that most phosphoguanides containing the amino benzimidazole have a high interaction tendency with COVID-19. Among them, compound 19 was identified as the strongest inhibitor with the -9.570 kcal/mol binding energy whereas, the binding energy of Remdesivir is -6.75 kcal/mol. The quantitative structure-activity relationship (QSAR) results demonstrated that the number of aromatic rings, amide's nitrogens and their ability in π -stacking, and hydrogen interactions with M^{pro} active sites are major factors contributing to the inhibitory activity of these compounds. Also, the NCI-RDG and DFT results were in good accordance with those of QSAR and molecular docking. The findings of this investigation can be underlying the synthesis of effective and efficient drugs against COVID-19.

© 2021 Elsevier B.V. All rights reserved.

1. Introduction

In recent months, the world has been facing a widespread illness known as "Coronavirus disease-2019 (COVID-19)" which has affected the global health and economy [1]. COVID-19 is a respiratory disease that might be causing fever, malaise, dry cough, pneumonia, and even to death [2,3]. There hasn't produced any safe and accepted medications to treat or prevent this infection yet [4]. Scientists around the world are attempting to achieve an effective drug for this global pressing problem [5,6]. Effective antiviral drugs based on phosphorus amide and phosphate with pyrazin and imidazole rings in their structure such as Adefovir, Foscarnet, Tenofovir, Sofosbuvir, Uprifosbuvir, and Remdesivir have been examined for the treatment of COVID-19 [7]. These drugs are efficient against Hepatitis, HIV, Influenza, and Ebola viral diseases [7]. Among these compounds, Remdesivir (GS-5734) was believed to be the most promising drug which can be used for treatment against COVID-19 [8]. This compound is a mono phosphoramidate prodrug

with a broad-spectrum antiviral activity against pneumoviruses, paramyxoviruses, filoviruses, and coronaviruses [8, 9], clinical tests are presently conducting to specify the complete efficacy of this prodrug in patients [10,11]. Recent studies reveal that the acting mechanism of the above-mentioned drugs is through inhibiting the main protease of the virus. Indeed, the inhibition potential of the main protease (M^{pro}) is the most hopeful drug target against coronaviruses [12–16]. The broadly used in modern drug design, molecular docking methods explore the ligand conformations adopted within the binding sites of macromolecular targets [17,18]. These procedures are logically successful for the prediction of binding affinity and have shown promising potential in facilitating drug design [19]. Hence, in this work, due to the need to discover new inhibitors and factors affecting M^{pro} inhibition, an attempt will be made to introduce new inhibitors based on phosphoramides with the higher COVID-19 M^{pro} inhibition potential than current acceptable drugs by molecular docking method. Many of synthetic and natural physiologically active compounds are of the guanidine and pyrazine motifs in their structures [20,21]. These bioactive compounds exhibit a variety of pharmaceutical properties such as anticancer agent [22], HIV protease inhibitor [23,24], anti-malarial [25], histamine H2 receptor antagonist [26], anti-hepatitis

* Corresponding author.

E-mail address: gholi_kh@modares.ac.ir (K. Gholivand).

¹ These authors contributed equally to this work.

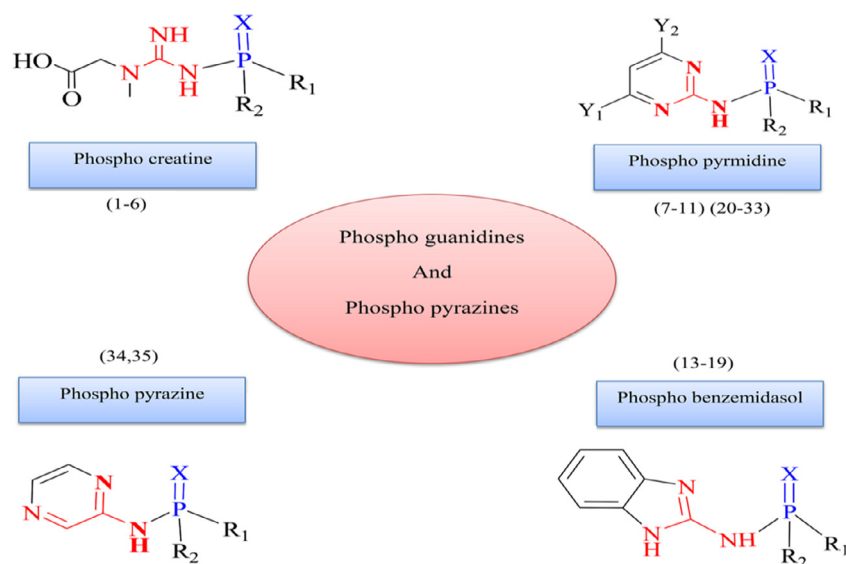


Fig. 1. General structure of the compounds studied.

[27], antimicrobial [28], fungicidal [29], anti-malarial [25], and anti-inflammatory [28]. Some research proves that phosphorylation of various drugs may be able to increase their biological activity [30]. There are compounds containing phospho guanidine and phospho pyrazine which represent agricultural and medicinal applications. Additionally, we have recently reported some of these compounds with both abilities to inhibit the acetylcholinesterase enzyme and low human toxicity [31–33]. Among the various phosphoramidate derivatives [31,33–35], we have studied phosphoguanidines and phosphopyrazines as effective compounds in drug design because of their extensive biological properties [31,33]. Due to the fact that Phosphoramidates are able to inhibit the main protease [36], In this work we selected 35 phosphoramidate compounds including the guanidine and pyrazine with the general formula $(R_1)(R_2)P(X)-Y$, that $X=O$ or S , $Y=$ creatine, amino pyrazine, amino benzimidazole, or amino pyrimidines, $R_1=(C_6H_5, OC_6H_5, OCH_3, \text{ or } OCH_2CH_3)$, and $R_2=(R, Y)$ (Fig. 1, Table 1). Molecular docking calculations are a beneficial tool to pave the way for drug discovery and saving resources and time for researchers. Hence, the Molecular docking study was performed to evaluate the efficacy of phosphoramidate based bioactive compounds against COVID-19 M^{Pro} . The identification of compounds (phosphobenzimidazoles and phosphopyrimidines) was reported as potent inhibitors of M^{Pro} by using the docking approach. The most efficient parameters affecting the inhibitory activity of the compounds were obtained through Quantitative structure-activity relationship (QSAR) studies with Genetic Algorithm-Artificial Neural Networks (GA-ANN). Also, Density Functional Theory (DFT) calculations including Frontier molecular orbitals, Reduced Density Gradient (RDG), molecular electrostatic potential (MEP) were used to verify docking and QSAR results.

2. Results and discussion

2.1. Structural analysis of docking

Since the main protease of severe acute respiratory syndrome coronavirus, M^{Pro} of SARS-CoV-2, has been identified as a suitable drug target to inhibition of this virus and COVID-19 [37,38], we have investigated the possible ways to inhibition of phosphoramidates against COVID-19 and also determined their orientation within the binding pocket of M^{Pro} . To achieve these goals, we performed the molecular docking of 35 titled compounds with the M^{Pro} of COVID-19.

The results of docking analysis indicated that compounds containing amino pyrimidine and amino benzimidazole substitutions have a higher inhibitory effect and lower binding energy than those containing creatine substitutions. Additionally, this class of compounds displays different trends to interact with protease, depending on the different attached substitutions to the phosphorus atom and pyrimidine rings (Fig. 2). The extracted data from the docking simulation such as free binding energy and inhibition constants (K_i) are presented in Table 2. Accordingly, the lowest and highest free binding energy belong to compounds 19 ($\Delta G_{\text{binding}} = -9.57$) and 5 ($\Delta G_{\text{binding}} = -4.02$), respectively. This indicates the high tendency of compound 19 to interact with the active sites of main protease of virus compared to other compounds. This tendency of 19 is bigger than some approved drugs such as Galidesivir, Remdesivir, Tenofovir, Sofosbuvir, and Ribavirin.

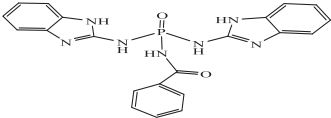
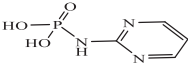
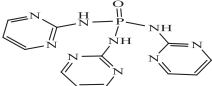
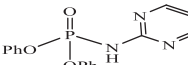
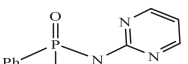

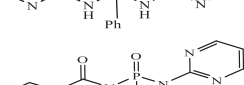
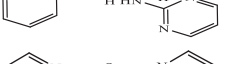
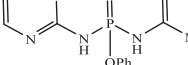
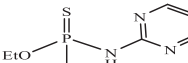
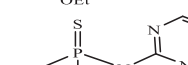
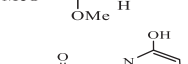
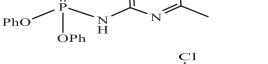
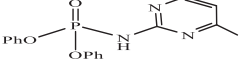
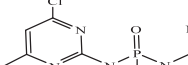
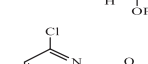
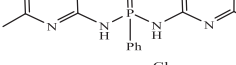
Obtained interactions from docking between some given molecules and M^{Pro} of COVID-19 are depicted in Fig. 2. Drawing a comparison between compounds in this figure reveals that, hydrogen bonding interactions are present in all ligand-protease complexes. Also, compounds 9, 10, 13–16, 19, and 29–32 are able to bind to the new coronavirus protease better than phosphoramidate antiviral drugs. In addition to hydrogen interactions, the mentioned compounds have π - π stacking, π -sulfur, and π -alkyl interactions. These interactions will increase as a result of increasing the number of aromatic substituents (Fig. 2). Comparing the interactions between compounds 15 and 19 with M^{Pro} , shows the effect of the nitrogen of amide and its ability to hydrogen interaction, which the binding affinity to the COVID-19 protease is enhanced by replacing the benzamide with phenyl group and increasing hydrogen interactions (Fig. 2E, F). The interaction model of compound 19 is depicted in Fig. 3 as illustrated, amide hydrogens and the carbonyl group of benzamide were involved in the formation of hydrogen bonds with Gln189, His164, and Glu166 residues from the active site of the M^{Pro} , respectively. Furthermore, aromatic rings were connected to Glu143, Cys145, and Met165 via π -Alkyl bonds and also to His163 and Cys145 residues through the π - π and π -sulfur interactions. These interactions have led to more stability of the target complex. In general, the connection desire of the inhibitors to COVID-19 protease depends on the position, size, volume, type of inhibitors' substituents, and their ability to form hydrogen interactions and π -stacking with active sites of the protease. In accordance with these studies and to obtain a rational relationship

Table 1
Docked and predicted binding energy values for phosphoguanidines and phosphopyrazines using GA-ANN.

No.	Structure	Ki	$\Delta G_{\text{binding}}$ (kcal/mol)	ΔG Pred. GA-ANN	ΔG Pred. LOO GA-ANN
1		10.46	-6.790	-6.53	-6.17
2		9.53	-6.850	-6.06	-6.15
3		106.93	-5.420	-5.96	-6.24
4		155.8	-5.190	-5.65	-5.56
5		1130	-4.020	-4.23	-4.39
6		458.11	-4.560	-4.42	-4.36
7		1.66	-7.890	-8.04	-8.14
8		1.13	-8.110	-7.82	-7.79
9		0.27149	-8.960	-8.90	-8.92
10		0.42244	-8.700	-8.66	-8.60
11		80.96	-5.580	-5.45	-5.42
12		126.82	-5.320	-5.40	-5.40
13		0.58149	-8.510	-8.43	-8.23
14		0.7948	-8.320	-8.42	-8.17
15		0.20594	-9.120	-9.27	-9.28
16		0.15927	-9.270	-9.47	-9.49
17		38.95	-6.020	-6.12	-6.24
18		62.04	-5.740	-5.82	-6.12

(continued on next page)

Table 1 (continued)

No.	Structure	Ki	$\Delta G_{\text{binding}}$ (kcal/mol)	ΔG Pred. GA-ANN	ΔG Pred. LOO GA-ANN
19		0.09676	-9.570	-9.54	-9.44
20		773.82	-4.240	-4.45	-4.56
21		4.95	-7.240	-7.32	-7.22
22		5	-7.230	-6.90	-6.79
23		8.12	-6.940	-7.49	-8.13
24		7.03	-7.030	-6.91	-6.90
25		1.39	-7.990	-7.73	-7.42
26		6.21	-7.100	-7.40	-7.32
27		173.36	-5.130	-4.94	-4.88
28		200.67	-5.040	-5.27	-5.22
29		1.04	-8.160	-8.00	-7.91
30		0.8069	-8.310	-7.77	-7.62
31		0.51533	-8.580	-8.79	-8.93
32		0.17826	-9.210	-8.56	-8.57
33		55.66	-5.800	-7.08	-7.86
34		392.75	-4.650	-4.45	-4.31
35		11.08	-6.760	-6.94	-6.84

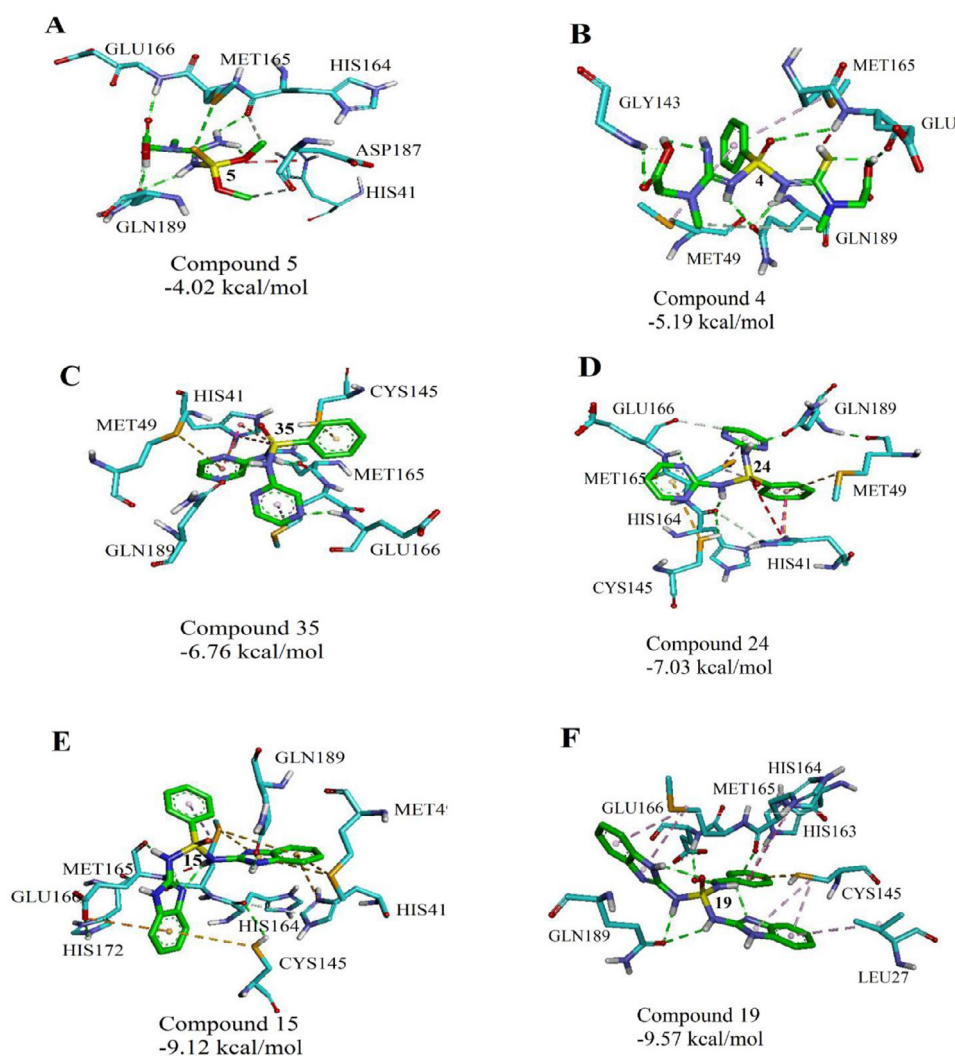


Fig. 2. Interactions established after docking the (A) 5, (B) 4, (C) 35, (D) 24, (E) 15, and (F) 19 against SARS-CoV-2. Inhibitors are in green, while the active protein pockets are light blue. The dotted lines illustrate various interactions between 19 and the active site residues, which including hydrogen bond (green), π -anion (Orange), π - π (Purple) and π -alkyl (pink) interactions.

between the structure and activity of compounds, the QSAR study was conducted.

2.2. QSAR analysis

QSAR calculations in the Genetic Algorithm and Artificial Neural Network (GA-ANN) method were conducted to specify the most important descriptors having an inhibitory activity against coronavirus 2019 (COVID-19). Seven descriptors, from total 175 structural and electrical descriptors, were selected as the most important descriptors in GA method which are the number of aromatic substituted carbons (nCaR), number of aromatic unsubstituted carbons (nCaH), number of nitrogens connected to phosphor (N-072), number of nitrogens of the aromatic ring (N-075), highest occupied molecular orbital (Homo), the effective charge on phosphor (Q_p), and molecular weight (Mv). These selected descriptors and the bonding energies obtaining from docking were chosen as input and output of ANN model, respectively. Obtained statistical parameters from this model include correlation coefficient ($R^2 = 0.9484$) and root mean square error (RMSE = 0.3665) which represent a nice correlation between dependent and independent variables and appropriate accuracy of the model were collected in Table 3. The predicted binding energies are listed in Table 1, and the relationship

between the predicted and the calculated values of the biological activity (binding energy) are shown in Fig. 4.

Cross-validation methods such as Leave-One-Out (LOO) and Leave-Multiple-Out (LMO) were also utilized to further validation of the performed model. In the former, one molecule acts as a prediction set and the other molecules develop the model, whereas, in the latter, some of the molecules (M) are considered as a prediction set. In LMO, it is supposed $M = 6$, and the L6O model is repeated 200 times. The LOO and L6O data have been shown in Table 3.

Fig. 5 reveal that the nCaR (the number of substituted aromatic carbons) and N-072 (the number of connected nitrogens to phosphor) are the most important parameters affecting the inhibitory behavior of the COVID-19.

The nCaR and nCaH molecular descriptors represent the number of substituted and unsubstituted aromatic carbons in which their presence in the structure of molecules gives useful information about the amount of hydrophobicity and hardness of compounds. Evaluating the impact of the aromatic rings on the inhibitory activity of subject compounds demonstrate that increasing the π -electron system or increasing the number of rings in the structure of inhibitors will be leading to an increase in the activity of the inhibitor. This increase is done by increasing the π - π in-

Table 2

The results obtained from docking analysis of COVID-19 main protease with 35 compounds.

No	$\Delta G_{\text{binding}}$ (kcal/mol)	Electrostatic Energy (kcal/mol)	vdW + Hbond + desolv Energy (kcal/mol)	Final Intermolecular Energy (kcal/mol)	Est. Inhibition Constant, Ki (μM)
1	-6.79	+0.15	-9.33	-9.18	10.46
2	-6.85	-0.14	-9.10	-9.24	9.53
3	-5.42	-0.72	-7.39	-8.10	106.93
4	-5.19	-0.36	-7.81	-8.18	155.8
5	-4.02	-0.28	-5.53	-5.81	1130
6	-4.56	-0.22	-6.72	-6.94	458.11
7	-7.89	-0.31	-8.77	-9.08	1.66
8	-8.11	-0.40	-9.50	-9.90	1.13
9	-8.96	-0.60	-9.85	-10.45	0.27149
10	-8.70	-0.62	-9.87	-10.49	0.42244
11	-5.58	-0.29	-7.08	-7.37	80.96
12	-5.32	-0.54	-5.97	-6.51	126.82
13	-8.51	-0.42	-9.88	-10.30	0.58149
14	-8.32	-0.33	-9.18	-9.51	0.7948
15	-9.12	-0.75	-9.86	-10.61	0.20594
16	-9.27	-0.80	-10.27	-11.06	0.15927
17	-6.02	-0.30	-7.51	-7.81	38.95
18	-5.74	-0.19	-6.74	-6.93	62.04
19	-9.57	-1.06	-10.29	-11.36	0.09676
20	-4.24	-0.87	-4.57	-5.44	773.82
21	-7.24	-3.81	-5.22	-9.03	4.95
22	-7.23	-0.38	-8.64	-9.02	5
23	-6.94	-0.35	-7.79	-8.14	8.12
24	-7.03	-0.78	-7.75	-8.52	7.03
25	-7.99	-0.80	-8.98	-9.78	1.39
26	-7.10	-0.73	-8.16	-8.89	6.21
27	-5.13	-0.68	-5.54	-6.23	173.36
28	-5.04	-0.69	-6.15	-6.83	200.67
29	-8.16	-0.50	-9.58	-10.08	1.04
30	-8.31	-0.37	-9.59	-9.96	0.8069
31	-8.58	-0.53	-9.70	-10.22	0.51533
32	-9.21	-0.57	-10.01	-10.58	0.17826
33	-5.80	-0.33	-7.12	-7.45	55.66
34	-4.65	-1.19	-4.65	-5.84	392.75
35	-6.76	-0.09	-8.04	-8.13	11.08
Adefovir	-4.18	-0.30	-6.27	-6.57	859.90
Foscarnet	-3.13	-2.04	-2.28	-4.32	512.5
Tenofovir	-4.97	-0.10	-10.24	-10.33	229.18
Sofosbuvir	-7.06	-0.50	-10.43	-10.94	6.71
Uprifosbuvir	-7.08	-0.14	-10.81	-10.96	6.47
Remdesivir	-6.75	-0.37	-11.46	-11.82	11.23

Table 3

Obtained statistical parameters from QSAR model.

	Training		Validation			
	R_t^2	RMSE _t	Q^2_{LOO}	RMSE _{LOO}	R^2_{L60}	RMSE _{L60}
GA-ANN	0.948	0.366	0.890	0.536	0.861	0.599

R_t^2 is a correlation coefficient of the training set; RMSE_t is a root mean square error of the training set; Q^2_{LOO} is a correlation coefficient of leave-one-out cross validation; RMSE_{LOO} is a root mean square error LOO-CV.

teractions between inhibitors and amino acid residues at the virus binding site.

Two other important and effective factors on inhibitory activity are N-072 and N-075 descriptors. Examination of these factors showed that as the number of nitrogens in the structure increased, the bonding energy decreased and the inhibitory power increased. Therefore, phosphorus-bonded nitrogens (amide nitrogens) have a greater and better effect on the virus than intra-ring nitrogen, due to their ability to form hydrogen bonds with the active sites of the COVID-19.

The HOMO orbitals of a chemical species are very important to define its reactivity [31]. And the greater its amount, the more reactive is the compound or the better interaction with the active site of the COVID-19 M^{Pro}.

Mv is one of the descriptors of this model, which displays the importance of molecular volume and molecule size in the inhibition mechanism. Indeed, a larger molecule can better interact with the connection sites and increase the hydrophobic nature of the molecules.

The effective charge on phosphorus is the last descriptor, which changes with the change of attached functional groups to the phosphorus atom. A survey of the relationship between the binding energy and charge on a phosphorus atom showed that the connected oxygen and sulfur to phosphorus atoms have a major effect on the charge on phosphorus atoms.

In order to better characterize the effects of N-072 and nCar descriptors on the structure of synthesized compounds and the inhibitory activity of compounds, we made a comparison between these descriptors and binding energies. As shown in Fig. 6, the results indicate that there is a logical relationship between these descriptors and binding energies. The studied compounds are classified into 5 categories; diamine benzimidazoles and substituted pyrimidinic diamines locate in the same category and have less binding energies and greater inhibitory activities than other groups. According to the diagram, aliphatic guanidine (creatine) and unsubstituted aromatic (amino pyrimidine) compounds with a lower number of heterocyclic rings, are of the highest binding energy. Another result is that compounds containing P=S have more bonding energy than compounds containing P=O, which could be

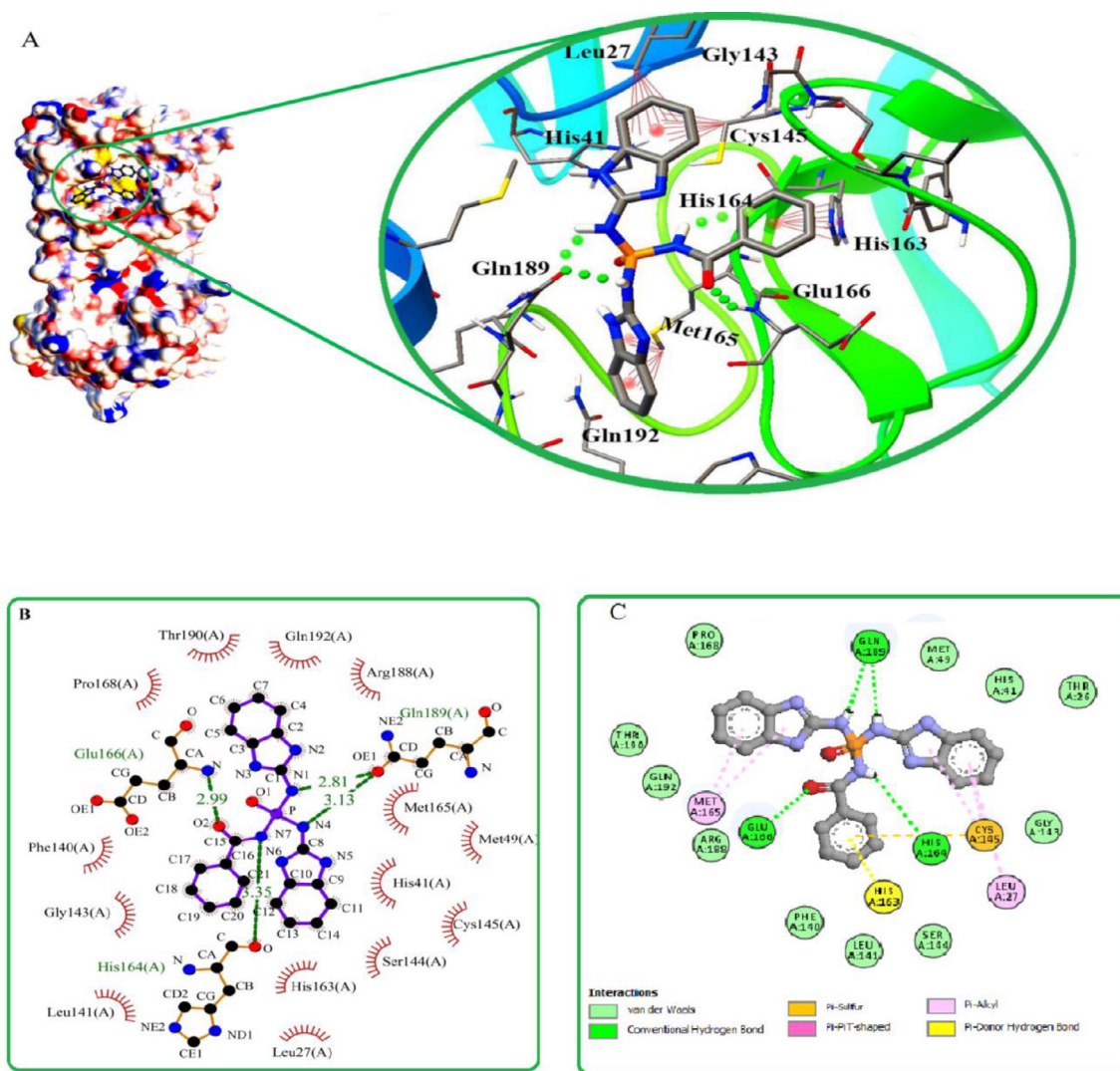


Fig. 3. Explaining different possible interactions of compound 19 with the main protease of COVID-19. (a) a 3D interaction diagram of 19 with the protease is shown in stick and surface models. The hydrogen bonds are shown in the form of green dots and the π -interactions are marked with red dotted lines. (b) And (c) 2D interaction diagram of 19 with the protease. Hydrogen bond interactions are indicated with green dashed lines.

attributed to differences in the model of their interaction with the enzyme.

2.3. Density functional theory calculations

In order to better understand the results of docking and QSAR studies on the more inhibition activity of derivatives containing both phosphoryl groups and aromatic systems in comparison to the compounds containing the thiophosphoryl and aliphatic group also determining the active sites in the structure of the molecules, their density functional theory (DFT) calculations including molecule electrostatic surface potential (MEP), frontier molecular orbitals (HOMO, LUMO), and reduced density gradient (RDG) were calculated.

2.3.1. Study of the molecular electrostatic potential (MEP) surfaces

The molecular electrostatic potential surfaces are extensively used in the analysis of the molecular stability, dipole moment, finding of the molecular active areas in electrophilic or nucleophilic reactions, hydrogen bonds, identifying the bioactive

molecules, and predicting applied sites [39]. Regarding the molecular overall charge distribution, each area on the surface has been recognized in different colors. In the following MEP maps, the red color represents the electron-rich zone and known as a nucleophilic center. The blue color is also attributed to electron-deficient areas and an electrophilic center. The regions between the two are shown by the yellow color, less electron-rich areas.

MEP maps of compounds 5 and 19 are calculated in the B3LYP/6-311+G** method and plotted in Fig. 7. In this Figure, the appearance of more positive and negative regions on potential surfaces reveal the reactivity for compound 19 (with the highest activity) higher than that of compound 5 (with the lowest activity). Oxygens bonded to phosphorus atoms are located in red areas and have a higher negative potential than sulfur atoms, indicating their strong tendency to participate in nucleophilic reactions. The blue areas describe the electropositive regions or electron deficiency areas that are located on the hydrogens attached to the nitrogen atoms and as electron acceptors supporting the interaction between the COVID-19 and the inhibitor. One more group which carries the most positive charge (yellow region) is the hydrogen atoms

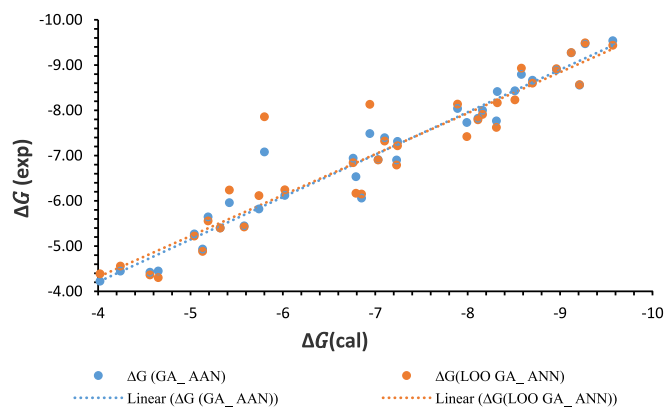


Fig. 4. The diagram of binding energy values from Docking versus the predicted binding energy values from the GA-ANN model for phospho guanidine compounds.

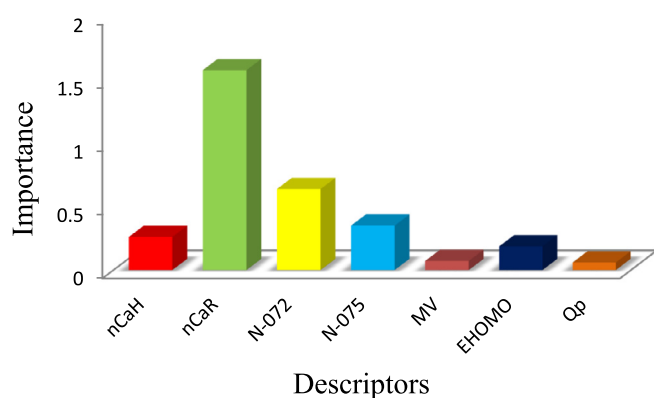


Fig. 5. The relative importance of selected descriptors in GA-ANN model.

attached to the aromatic rings. These moieties exhibited $\pi \cdots \pi$ interactions with the aromatic residues of the active site due to the accumulation of positive potential.

2.3.2. Frontier molecular orbitals

The analysis of Frontier molecular orbitals of compounds is one of the methods used to predict reactive electrophilic or nucleophilic sites. The highest occupied molecular orbital (HOMO) and the lowest unoccupied molecular orbital (LUMO) are called frontier molecular orbitals. The energy values of HOMO and LUMO orbitals and their energy gap provide information about the biolog-

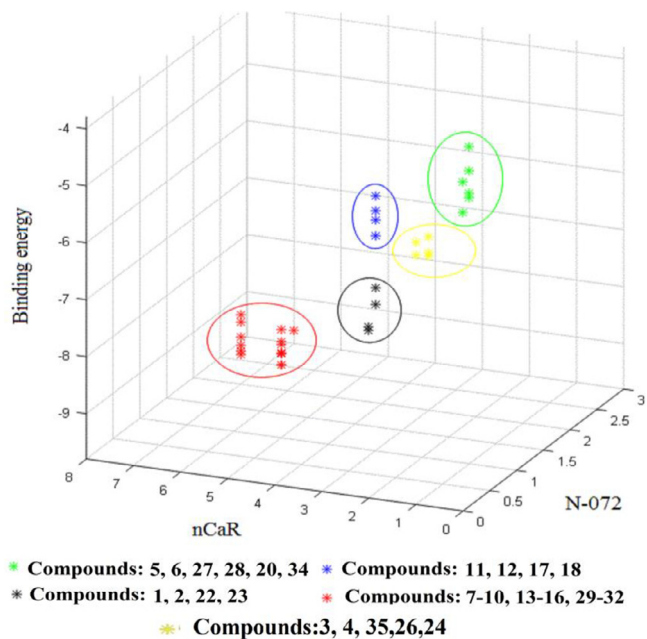


Fig. 6. The relationship and changes in the binding-energy values of all understudied compounds compared to N-072 and nCaR variables, green star: derivatives of thio phospho guanidine and diphenylphosphinic amide containing the aromatic unsubstituted carbons, blue star: derivatives of thio phospho guanidine containing the aromatic substituted carbons, yellow star: derivatives of diphenyl (guanidine) phosphoramidate and guanidine diphenylphosphinic amide containing the aromatic unsubstituted carbons, black star: derivatives of bis(guanidine) phenylphosphonic diamide and bis(guanidine)phenylphosphor amidate containing the aromatic unsubstituted carbons, red star: derivatives of bis(guanidine) phenylphosphonic diamide, bis(guanidine)phenylphosphor amidate, diphenyl (guanidine) phosphoramidate, and guanidine diphenylphosphinic amide containing the aromatic substituted carbons.

ical activity of the compounds [40]. Compounds that have a small energy gap are more polarizable and generally more chemical reactivity [41]. HOMO-LUMO energies of compounds were calculated using DFT at B3LYP method and 6-311+G** basis set. Also, HOMO-LUMO orbitals composition analysis of compounds 5 and 19 were obtained by the Hirshfeld method via the Multiwfn 3.7 program [42]. HOMO-LUMO plots of the mentioned compounds with their contribution percent gathered in Fig. 8. HOMO-LUMO gap energies of compounds 5 and 19 calculated 4.584 eV and 2.971 eV respectively, these values are comparable with the bandgap energy values of the bioactive molecules [21,43,44]. The results represent that the

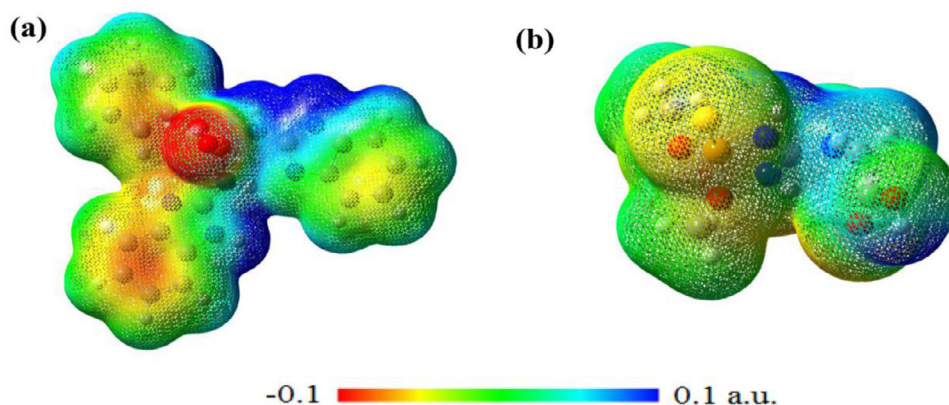


Fig. 7. Three-dimensional map of the molecular electrostatic potential of compounds 19 (a) and 5 (b). The red and blue regions show the electron-rich and the electron-deficient areas, respectively.

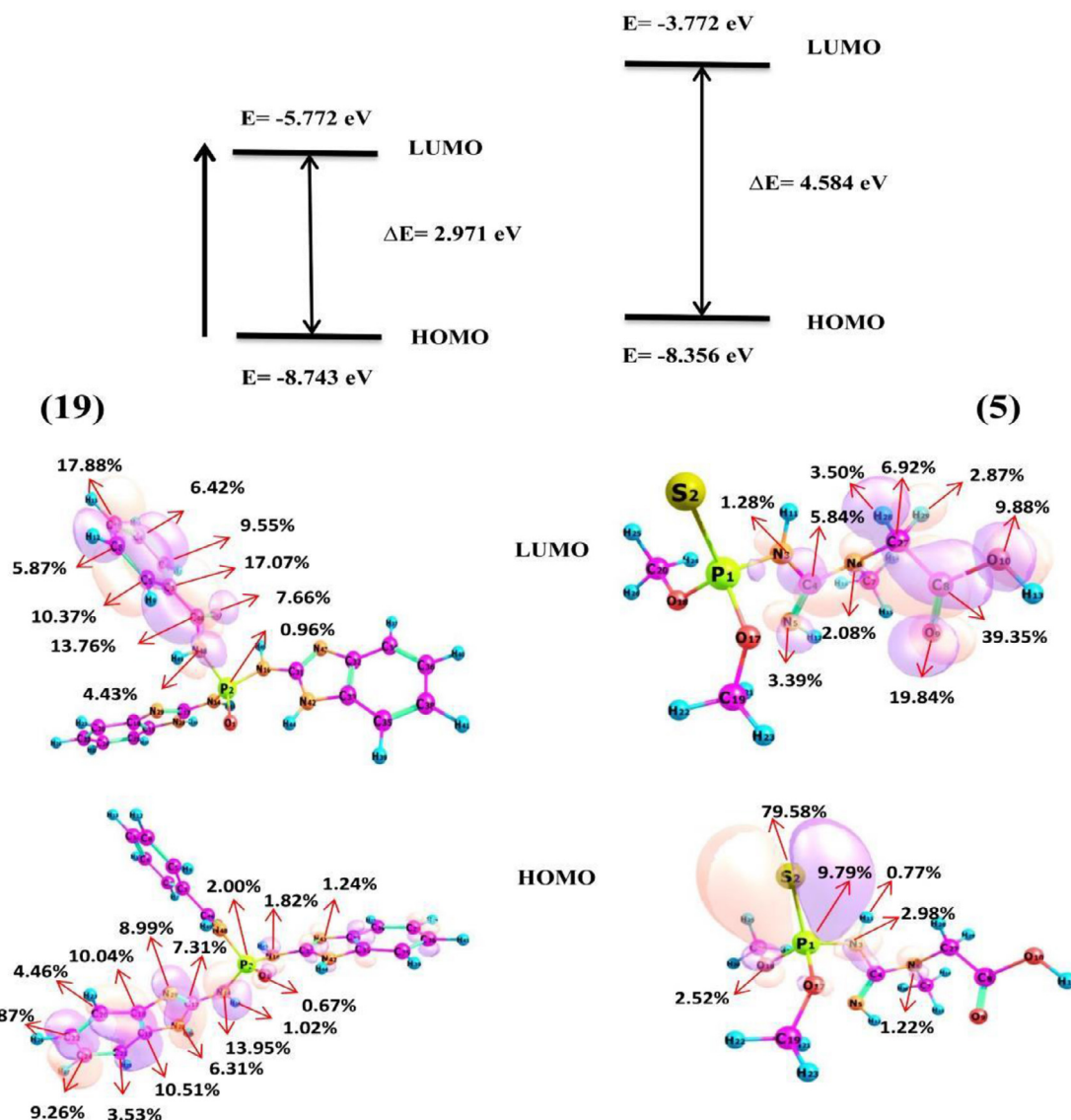


Fig. 8. HOMO-LUMO orbitals composition analysis of compounds 5 and 19 were obtained by the Hirshfeld method via the Multiwfn program.

frontier orbitals bandgap of 19 is smaller than 5 which is evidence of stronger interaction with the main protease of Covid-19.

Reactivity descriptors such as Ionization potential (IP), Electron affinity (EA), Chemical hardness (η) and Softness (S), chemical potential (μ), and Electrophilicity index (ω) are descriptors used to predict a drug's tendency to engage in Drug-acceptor interactions and also, to explain their properties and chemical activities [45]. The values of Global molecular reactivity descriptors of compound 19 were calculated using HOMO and LUMO energies from the following relationships, Table 4:

$$\text{Ionization potential}(IP) = -E_{HOMO}. \quad (1)$$

$$\text{Electron affinity}(EA) = -E_{LUMO} \quad (2)$$

$$\text{Electronegativity}(\chi) = (IP + EA)/2 \quad (3)$$

$$\text{Chemical Potential}(\mu) = -\chi \quad (4)$$

$$\text{Chemical hardness}(\eta) = (IP - EA)/2 \quad (5)$$

Table 4

Obtained Reactivity descriptors of compound 19 from DFT calculations.

compound	19
Ionization potential (IP)	8.743 eV
Electron affinity (EA)	5.772 eV
Electronegativity (χ)	7.257 eV
Chemical Potential (μ)	-7.257 eV
Chemical hardness (η)	1.485 eV
Chemical softness (S)	0.673 eV
Electrophilicity index(ω)	17.728 eV
Energy change (ΔE)	-17.728eV
Maximal charge acceptance(ΔN_{max})	4.886 eV
$\Delta E/\Delta N_{max}$	-3.629 eV

$$\text{Chemical softness}(S) = 1/\eta \quad (6)$$

$$\text{Electrophilicity index}(\omega) = \mu^2/2\eta \quad (7)$$

$$\text{Energy change}(\Delta E) = -\mu^2/2\eta \quad (8)$$

$$\text{Maximal charge acceptance}(\Delta N_{max}) = -\mu/\eta \quad (9)$$

With regard to the direct relationship between ionization potential and electrophilicity with HOMO and LUMO energies, respectively. The *IP* and *EA* values of 19 show that 8.743 eV of energy is required to removing electrons from HOMO. On the other hand, the low value of electrophilicity (5.772 eV) indicates its greater tendency to interact with nucleophiles. The values of chemical harness (η) and electron transition energy (ΔE) have been calculated 1.485 eV and -17.728 eV, respectively. With respect to the fact that whenever $\eta > 0$ and $\Delta E < 0$, the charge transition process is desirable in terms of energy [46], the desirability of these values for compound 19 indicates its tendency to interact with the COVID-19 acceptor as a bioactive molecule. If the ratio between the energy changes and the maximum charge acceptance is zero ($\Delta E / \Delta N_{max} = 0$), it will indicate that the compound is electron saturated and has no tendency to participate in the charge transfer process [47]. This value for compound 19 is calculated -3.629 which indicated its ability to charge transfer and interact with the acceptor.

2.3.3. Reduced density gradient (RDG)

Reduced density gradient (RDG) is a non-dimensional principal quantity based on electron density $\rho(r)$ and its first derivation. This highly efficient method to analyze weak interactions has been developed by Johnson et al. [48].

$$RDG(r) = \frac{1}{2(3\pi^2)^{1/3}} \frac{\nabla\rho(r)}{\rho(r)^{4/3}} \quad (10)$$

In order to better imagination of interactions, RDG plots related to compounds 5, 16, and 19 were plotted using Multiwfn 3.7 [42] and VMD 1.9.3 [49] softwares in Fig. 9. In RDG analysis, RDG clusters, Reduced Density Gradient spikes, and λ_2 give some information about the type of bond and the strength of the interaction. The van der Waals interactions show values close to zero of λ_2 and density ($\rho \approx 0$, $\lambda_2 \approx 0$), while the areas of strong repulsive interactions are known with a large positive of λ_2 and high values of density ($\rho > 0$, $\lambda_2 > 0$) and hydrogen interactions show large negative values of λ_2 with high values of density ($\rho > 0$, $\lambda_2 < 0$) [48,50]. According to Fig. 9, different interactions were distinguished by different colors, in which the red color indicates the steric repulsion between the oxygen atoms of the methoxy substituents in compound 5 and within the phenyl and imidazole 19 and 16 rings. The green color indicates the Van der Waals interactions and the blue area is known as strong hydrogen interactions. As can be seen, in compound 5, the van der Waals interaction is the dominant interaction in this molecule, but in 16 and 19, in addition to the previous interaction, there are strong hydrogen interactions. The results of these studies are in good accordance with the results of the docking studies.

3. Conclusion

In this study, the aim was to find compounds with a higher potential of inhibiting COVID-19 M^{pro} than the current acceptable drugs. For this reason, we have undertaken docking, QSAR, and other computational investigations on 35 phosphoramidate compounds based on the guanidine and pyrazines against COVID-19 M^{pro} . One of which (19) showed remarkable binding interactions with the target better than the Remdesivir. This compound is a mono phosphoramidate based on the benzimidazole with anti-acetylcholinesterase activity. In general, the compounds containing amino pyrimidine and amino benzimidazole substitutions had a higher inhibitory effect and lower binding energy than the derivatives containing creatine substitutions. QSAR calculation results using the Artificial Neural Network (GA-ANN) method reveal that the number of aromatic substituted carbons (*nCaR*), aromatic unsubstituted carbons (*nCaH*), nitrogens connected to phosphor (*N-072*),

nitrogens of the aromatic ring (*N-075*), energies of highest occupied molecular orbital (*HOMO*), the effective charge on phosphor (Q_p) and molecular volume (*Mv*) descriptors are the most significant parameters influencing the inhibitory activity. The DFT calculations including molecule electrostatic surface potential (MEP), frontier molecular orbitals (HOMO, LUMO), and reduced density gradient (RDG) were used to verify docking and QSAR. The outcomes of these calculations confirmed the relationship between electronic properties and the desire of inhibitors to connect the M^{pro} .

Taken together, this study help to gain a better understanding of the interactions between the COVID-19 main protease and its inhibitors, which in turn assist in the exploration, develop and design of the anti-coronavirus drugs.

4. Materials and methods

4.1. Data set

In sum, 35 phosphoramides containing guanidine substitutions (including creatine and pyrimidine and the amino benzimidazole) and pyrazine substitution were selected among our previously reported data (Table 1) [31]. The toxicity of these compounds to humans has been investigated by measuring the anti-acetylcholinesterase activity. The mentioned compounds have been studied as antiviral agents for COVID-19 via docking, QSAR, and MEP.

4.2. Protocol of docking study

In order to investigate the conformation and determine the orientation of the compounds within the active site of the enzyme, molecular docking was performed using Auto Dock 4.2 software. The crystal structure of the COVID-19 (PDB ID: 6LU7) was used in this study [6].

To prepare proteins and ligands, firstly, the structures of all inhibitors were fully optimized at the B3LYP / 6-311 G ** level of DFT theory [51]. All the water molecules were removed from the protein structure and hydrogens were added to the structure. One hundred docking runs through Lamarckian genetic algorithm were performed and According to the default settings, the docking parameters were set. Results that less differ than 0.5 Å in Root Mean Square Deviation (RMSD) to each other were clustered together then, these optimized clusters based on the lowest binding energy were ranked. Finally, the cluster which has the lowest binding energy and the highest number of conformations was selected as the best-docked conformation.

According to the Eq. (11), Free Gibbs energy calculated using AutoDock4.2 and to show the 2D enzyme-ligand interaction, the Ligplot (v.1.4.5) software was utilized [52]. View of docking results and analysis of their levels were achieved from the graphical display by AutoDock Tools and Discovery studio visualizer software [53].

$$\Delta G_{binding} = [\Delta G_{intermolecular} + \Delta G_{internal} + \Delta G_{torsional}] - [\Delta G_{unbound}] \quad (11)$$

4.3. Descriptors calculation for QSAR

Constructing numerical descriptors of a set of molecules to build QSAR models is essential. A descriptor can represent a quantitative property that depends on the structure of the molecule [51]. The uncertainty of experimental measurements has no effect on theoretical descriptors, so one can calculate them for not synthesized compounds. A large number of molecular descriptors were calculated via HyperChem, Dragon, [54] and Gaussian 03 [55].

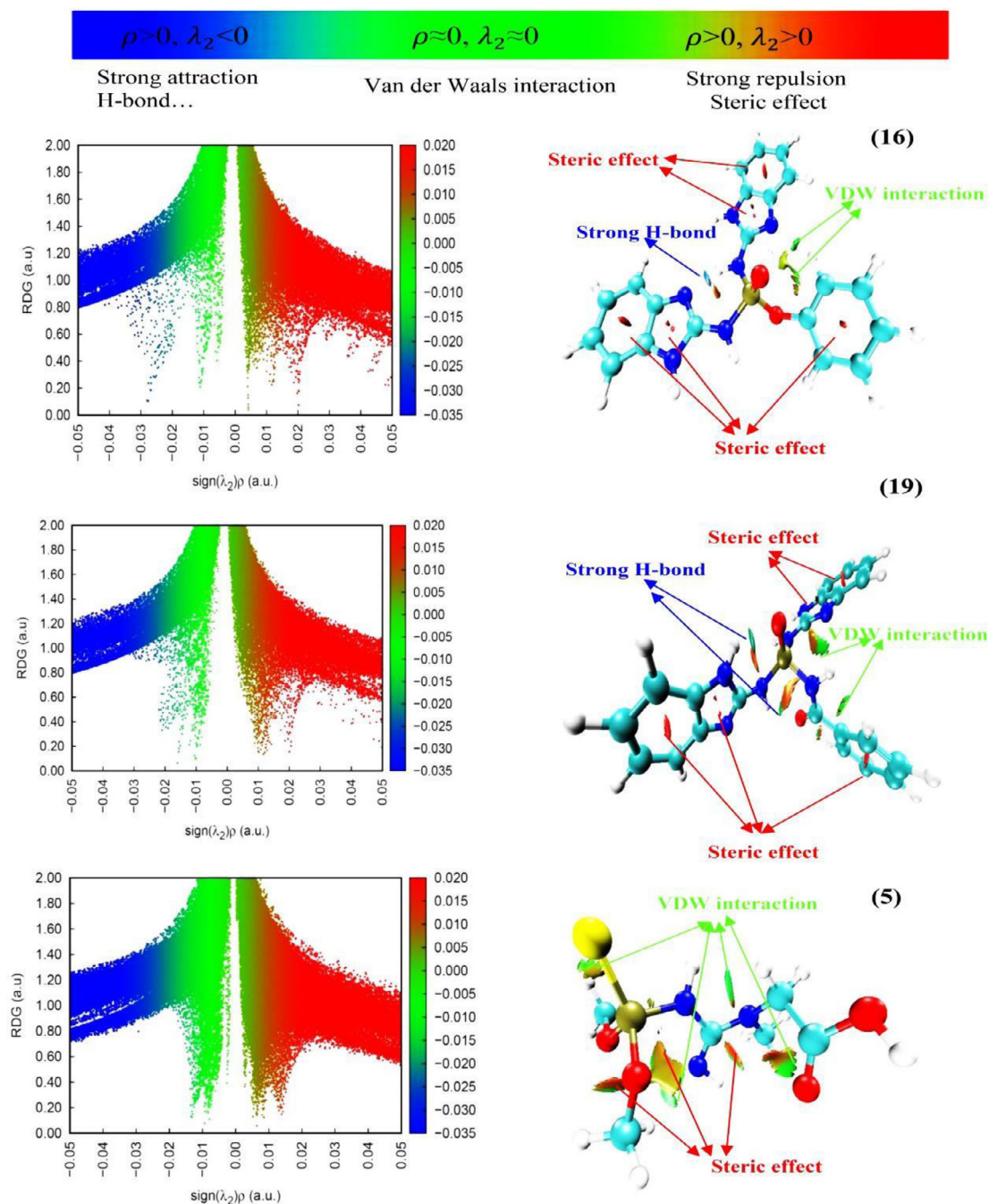


Fig. 9. Interactions, RDG plots related to compounds 5, 16, and 19 were plotted using Multiwfn and VMD softwares.

Some chemical parameters including hydrophobic coefficient (Log P), and molecular polarizability (MP) were calculated using HyperChem software. Different functional groups, topological, geometrical and constitutional descriptors for each molecule were calculated by Dragon software. Gaussian 03 was also employed for calculation of different quantum chemical descriptors including, energies of highest occupied molecular orbital ($HOMO$), lowest unoccupied molecular orbital ($LUMO$), the energy difference between $LUMO$ and $HOMO$ (ΔE_{L-H}), dipole moment (DM), charges on atoms (Q_i) and total energy (E), electrophilicity (ω), molecular volume (Mv), polarizability (PL , the charge difference between the atoms in functional groups), electronic chemical potential (μ), chemical hardness (η), Chemical softness (S), and chemical power ($C\pi$) [35,56].

Generally, by removing descriptors that have the same values for all molecules as well as removing some descriptors that have a greater correlation coefficient than 0.90, only 87 descriptors were used in QSAR studies. The calculated values of some descriptors for each compound are listed in Tables 5 and S1).

4.4. Chemometric methods

Since nonlinear methods consider both linear and nonlinear properties between dependent and independent variables, nonlinear ones are more suitable for selecting descriptors [55]. In this work, the correlation between binding energy and structural properties was achieved using a genetic algorithm-artificial neural network (GA-ANN) in MATLAB software (version 8.5.0 (R2015a)). The

Table 5
Quantum-chemical and geometrical descriptors for 35 compounds.

Electronic												
No.	Q _p (a.u)	Q _{N(1)}	Q _{C(1)}	Q _{N(2)}	Q _{p(x)}	PL _(P=0)	PL _{P-N}	PL _{N1-H}	PL _{C=N}	E _{HOMO} (ev)	E _{LUMO}	
1	2.450	-0.976	0.625	-0.739	-1.022	-3.472	-3.426	1.399	-1.364	-8.786	-5.239	
2	2.040	-0.980	0.627	-0.712	-1.063	-3.103	-3.020	1.388	-1.339	-8.774	-5.692	
3	2.387	-0.972	0.642	-0.763	-1.017	-3.404	-3.359	1.393	-1.405	-8.878	-4.932	
4	2.210	-0.972	0.650	-0.750	-1.052	-3.262	-3.182	1.392	-1.400	-8.761	-5.473	
5	0.210	-0.429	-0.354	-0.334	-0.248	-0.458	-0.639	0.763	0.020	-8.356	-3.772	
6	1.981	-1.000	0.624	-0.700	-0.603	-2.584	-2.981	1.420	-1.324	-8.374	-3.781	
7	2.448	-0.944	0.620	-0.541	-1.031	-3.479	-3.392	1.384	-1.161	-9.248	-5.220	
8	2.042	-0.947	0.620	-0.339	-1.057	-3.099	-2.989	1.372	-0.959	-9.278	-5.673	
9	2.175	-0.930	0.629	-0.547	-1.038	-3.213	-3.105	1.354	-1.176	-9.147	-5.493	
10	2.385	-0.937	0.624	-0.540	-1.031	-3.416	-3.322	1.371	-1.164	-9.153	-5.223	
11	1.941	-0.958	0.614	-0.539	-0.530	-2.471	-2.899	1.391	-1.153	-8.369	-5.121	
12	1.931	-0.961	0.613	-0.539	-0.524	-2.455	-2.892	1.396	-1.152	-8.377	-5.122	
13	2.454	-0.971	0.587	-0.578	-1.023	-3.477	-3.425	1.384	-1.165	-8.857	-5.224	
14	2.049	-0.971	0.588	-0.548	-1.081	-3.130	-3.020	1.403	-1.136	-8.744	5.574	
15	2.174	-0.936	0.612	-0.574	-1.028	-3.202	-3.110	1.345	-1.186	-8.696	-5.519	
16	2.376	-0.959	0.604	-0.572	-1.008	-3.384	-3.335	1.374	-1.176	-8.752	-5.213	
17	1.553	-0.822	0.575	-0.559	-0.380	-1.933	-2.375	1.253	-1.134	-7.279	-5.048	
18	1.516	-0.825	0.567	-0.508	-0.374	-1.890	-2.341	1.264	-1.075	-7.299	-5.053	
19	2.380	-0.757	0.561	-0.422	-1.023	-3.403	-3.137	0.757	-0.983	-8.743	-5.772	
20	2.403	-0.940	0.615	-0.509	-1.019	-3.422	-3.343	1.371	-1.124	-9.224	-5.275	
21	2.334	-0.977	0.609	-0.508	-1.036	-3.370	-3.311	1.446	-1.117	-9.056	-5.257	
22	2.448	-0.942	0.606	-0.514	-1.029	-3.477	-3.390	1.383	-1.120	-9.254	-5.236	
23	2.040	-0.948	0.607	-0.516	-1.054	-3.094	-2.988	1.373	-1.123	-9.292	-5.675	
24	2.171	-0.929	0.614	-0.515	-1.033	-3.204	-3.100	1.354	-1.129	-9.158	-5.498	
25	2.304	-0.949	0.613	-0.561	-1.007	-3.311	-3.253	1.414	-1.174	-9.158	-5.743	
26	2.382	-0.935	0.609	-0.511	-1.026	-3.408	-3.317	1.371	-1.120	-9.162	-5.275	
27	1.940	-0.947	0.608	-0.511	-0.553	-2.493	-2.887	1.385	-1.119	-8.353	-5.249	
28	1.949	-0.947	0.608	-0.512	-0.560	-2.509	-2.896	1.384	-1.120	-8.352	-5.246	
29	2.448	-0.940	0.625	-0.547	-1.029	-3.477	-3.388	1.364	-1.172	-9.182	-5.220	
30	2.445	-0.934	0.624	-0.535	-1.024	-3.469	-3.379	1.376	-1.159	-8.513	-5.225	
31	2.380	-0.932	0.624	-0.534	-1.012	-3.392	-3.312	1.365	-1.158	-8.510	-5.206	
32	2.170	-0.924	0.631	-0.536	-1.029	-3.199	-3.094	1.351	-1.167	-8.506	-5.502	
33	2.456	-0.927	0.625	-0.529	-1.030	-3.486	-3.383	1.370	-1.154	-8.378	-5.226	
34	2.404	-0.928	0.441	-0.597	-1.018	-3.422	-3.332	1.344	-1.038	-9.336	-5.031	
35	2.182	-0.966	0.362	-0.474	-1.050	-3.232	-3.148	1.383	-0.836	-8.940	-5.536	

best selected-descriptors utilizing a genetic algorithm (GA) have been used as input variables for the development of an artificial neural network (ANN) model. In the GA-ANN method, ANN is used as a fitness approximation and GA to perform robust and effective evolutionary optimization. The theory of this method has been adequately described elsewhere [57].

In order to evaluate the generated models, the parameters of the correlation coefficient (R), root mean square error (RMSE), leave-one-out cross-validation (LOO-CV), and Leave-multiple-out cross-validation (LMO-CV) approaches were used. In LOO-CV, one compound is removed at each step as a prediction set and the model is developed using the remaining molecules as the training set. Also, a group of six compounds randomly selected to perform the authentication method of leave-6-out (L6O) cross-validation.

Declaration of Competing Interest

The authors declare no conflict of interest.

CRediT authorship contribution statement

Khodayar Gholivand: Conceptualization. **Fahimeh Mohammadpanah:** Methodology, Formal analysis, Writing – original draft. **Mahsa Pooyan:** Software, Resources, Validation, Investigation. **Roohollah Roohzadeh:** Visualization, Software, Writing – review & editing.

Acknowledgements

We would like to thank our colleagues from the University of Tarbiat Modares who provided valuable insights.

Supplementary materials

Supplementary material associated with this article can be found, in the online version, at [doi:10.1016/j.molstruc.2021.131481](https://doi.org/10.1016/j.molstruc.2021.131481).

References

- [1] WH. Organization, Coronavirus disease (COVID-19) Situation Report – 121, World Health Organization (WHO), Geneva, 2020.
- [2] C. Huang, Y. Wang, X. Li, L. Ren, J. Zhao, Y. Hu, L. Zhang, G. Fan, J. Xu, X. Gu, Clinical features of patients infected with 2019 novel Coronavirus in Wuhan, China, *Lancet* 395 (2020) 497–506.
- [3] N. Zhu, D. Zhang, W. Wang, X. Li, B. Yang, J. Song, X. Zhao, B. Huang, W. Shi, R. Lu, et al., A novel coronavirus from patients with pneumonia in China, 2019, *N. Engl. J. Med.* 382 (2020) 727–733.
- [4] A. Lassoued, AB Saad, H. Lassoued, R. Ketata, O. Boubaker, Dataset on the COVID-19 Pandemic Situation in Tunisia with Application to SIR Model, *medRxiv PPR:* (2020) R155789.
- [5] K.T. Choy, A.Y.L. Wong, P. Kaewpreedee, S.F. Sia, D. Chen, K.P.Y. Hui, D.K.W. Chu, M.C.W. Chan, P.P.H. Cheung, X. Huang, Remdesivir, lopinavir, emetine, and Homoharringtonine Inhibit SARS-CoV-2 Replication *in vitro*, *Antivir. Res.* 178 (2020) 104786.
- [6] Z. Jin, X. Du, Y. Xu, Y. Deng, M. Liu, Y. Zhao, B. Zhang, X. Li, L. Zhang, C. Peng, et al., Structure of M^{pro} from SARS-CoV-2 and discovery of its inhibitors, *Nature* 582 (2020) 289–293.
- [7] B. Shah, P. Modi, S.R. Sagar, *In silico* studies on therapeutic agents for COVID-19: drug repurposing approach, *Life Sci.* 252 (2020) 117652.
- [8] A.J. Brown, J.J. Won, R.L. Graham, K.H. Dinnon, A.C. Sims, J.Y. Feng, T. Cihlar, M.R. Denison, R.S. Baric, T.P. Sheahan, Broad spectrum antiviral remdesivir inhibits human endemic and zoonotic deltacoronaviruses with a highly divergent RNA dependent RNA polymerase, *Antivir. Res.* 169 (2019) 104541.

- [9] T.P. Sheahan, A.C. Sims, R.L. Graham, V.D. Menachery, L.E. Gralinski, J.B. Case, S.R. Leist, K. Pyrc, J.Y. Feng, I. Trantcheva, et al., Broad-spectrum antiviral GS-5734 inhibits both epidemic and zoonotic coronaviruses, *Sci. Transl. Med.* 9 (396) (2017) 1–10.
- [10] Adaptive COVID-19 Treatment Trial. ClinicalTrials.gov identifier: NCT04280705. Posted February 21, 2020. Accessed March 19, 2020. Available at: <https://clinicaltrials.gov/ct2/show/NCT04280705?term=remdesivir&cond=covid-19&draw=2&rank=5>.
- [11] M. Wang, R. Cao, L. Zhang, X. Yang, J. Liu, M. Xu, Z. Shi, Z. Hu, W. Zhong, G. Xiao, Remdesivir and chloroquine effectively inhibit the recently emerged novel coronavirus (2019-nCoV) in vitro, *Cell Res.* 30 (2020) 269–271.
- [12] J.E. Blanchard, N.H. Elowe, C. Huitema, P.D. Fortin, J.D. Cechetto, L.D. Eltis, E.D. Brown, High-throughput screening identifies inhibitors of the SARS coronavirus main proteinase, *Chem. Biol.* 11 (2004) 1445–1453.
- [13] C. Chu, V. Cheng, I. Hung, M. Wong, K. Chan, K. Chan, R. Kao, L. Poon, C. Wong, Y. Guan, Role of lopinavir/ritonavir in the treatment of SARS: initial virological and clinical findings, *Thorax* 59 (2004) 252–256.
- [14] L.L. Lu, N. Mahindroo, P.H. Liang, Y.H. Peng, C.J. Kuo, K.C. Tsai, H.P. Hsieh, Y.S. Chao, S.Y. Wu, Structure-based drug design and structural biology study of novel nonpeptide inhibitors of severe acute respiratory syndrome coronavirus main protease, *J. Med. Chem.* 49 (2006) 5154–5161.
- [15] A.T. Ton, F. Gentile, M. Hsing, F. Ban, A. Cherkaev, Rapid identification of potential inhibitors of SARS-CoV-2 main protease by deep docking of 1.3 billion compounds, *Mol. Inform.* 39 (2000028) (2020) 1–7.
- [16] A. Zumla, J.F. Chan, E.I. Azhar, D.S. Hui, K.Y. Yuen, Coronaviruses–drug discovery and therapeutic options, *Nat. Rev. Drug Discov.* 15 (2016) 327–347.
- [17] A.C. Anderson, The process of structure-based drug design, *Chem. Biol.* 10 (2003) 787–797.
- [18] L.G. Ferreira, R.N. Dos Santos, G. Oliva, A.D. Andricopulo, Molecular docking and structure-based drug design strategies, *Molecules* 20 (2015) 13384–13421.
- [19] A. Abdolmaleki, J.B. Ghasemi, F. Ghasemi, Computer aided drug design for multi-target drug design: SAR/QSAR, molecular docking and pharmacophore methods, *Curr. Drug Targets* 18 (2017) 556–575.
- [20] R.G. Berlinck, Natural guanidine derivatives, *Nat. Prod. Rep.* 19 (2002) 617–649.
- [21] K. Shalini, P.K. Sharma, N. Kumar, Imidazole and its biological activities: a review, *Der Chem. Sin.* 1 (2010) 36–47.
- [22] K. Ohara, M. Smietana, A. Restouin, S. Mollard, J.P. Borg, Y. Collette, J.J. Vasseur, Amine-guanidine switch: a promising approach to improve DNA binding and antiproliferative activities, *J. Med. Chem.* 50 (2007) 6465–6475.
- [23] A. Kanwal, M. Ahmad, S. Aslam, S.A.R. Naqvi, M.J. Saif, Recent advances in antiviral benzimidazole derivatives: a mini review, *Pharm. Chem. J.* 53 (2019) 179–187.
- [24] M. Zhu, L. Ma, H. Zhou, B. Dong, Y. Wang, Z. Wang, J. Zhou, G. Zhang, J. Wang, C. Liang, Preliminary SAR and biological evaluation of potent HIV-1 protease inhibitors with pyrimidine bases as novel P2 ligands to enhance activity against DRV-resistant HIV-1 variants, *Eur. J. Med. Chem.* 185 (2020) 111866.
- [25] Y. Younis, F. Douelle, D. González Cabrera, C. Le Manach, A.T. Nchinda, T. Paquet, L.J. Street, K.L. White, K.M. Zabiulla, J.T. Joseph, Structure-activity-relationship studies around the 2-amino group and pyridine core of antimalarial 3, 5-diarylaminopyridines lead to a novel series of pyrazine analogues with oral in vivo activity, *J. Med. Chem.* 56 (2013) 8860–8871.
- [26] S. Pockes, D. Wifling, M. Keller, A. Buschauer, S. Elz, Highly potent, stable, and selective dimeric hetarylpropylguanidine-type histamine H2 receptor agonists, *ACS Omega* 3 (2018) 2865–2882.
- [27] W. Yu, C. Goddard, E. Clearfield, C. Mills, T. Xiao, H. Guo, J.D. Morrey, N.E. Motter, K. Zhao, T.M. Block, Design, synthesis, and biological evaluation of triazolo-pyrimidine derivatives as novel inhibitors of hepatitis B virus surface antigen (HBsAg) secretion, *J. Med. Chem.* 54 (2011) 5660–5670.
- [28] A.A. Kadi, N.R. El-Brollosy, O.A. Al-Deeb, E.E. Habib, T.M. Ibrahim, A.A. El-Emam, Synthesis, antimicrobial, and anti-inflammatory activities of novel 2-(1-adamantyl)-5-substituted-1, 3, 4-oxadiazoles and 2-(1-adamantylamino)-5-substituted-1, 3, 4-thiadiazoles, *Eur. J. Med. Chem.* 42 (2007) 235–242.
- [29] X.J. Zou, L.H. Lai, G.Y. Jin, Z.X. Zhang, Synthesis, fungicidal activity, and 3D-QSAR of pyridazinone-substituted 1, 3, 4-oxadiazoles and 1, 3, 4-thiadiazoles, *J. Agric. Food Chem.* 50 (2002) 3757–3760.
- [30] V.R. Katla, R. Syed, C.S. Kuruva, H.K. Kuntapakam, N.R. Chamarthi, Synthesis of novel phosphorylated guanidine derivatives from cyanamide and their anti-inflammatory activity, *Chem. Pharm. Bull.* 61 (2013) 25–32.
- [31] K. Gholivand, F. Mohammadpanah, M. Pooyan, A.A.E. Valmoozi, M. Sharifi, A. Mani-Varnosfaderani, Z. Hosseini, Synthesis, crystal structure, insecticidal activities, molecular docking and QSAR studies of some new phospho guanidines and phospho pyrazines as cholinesterase inhibitors, *Pestic. Biochem. Physiol.* 157 (2019) 122–137.
- [32] N. Inguibert, L. Jäger, M. Taillefer, H.J. Cristau, Synthesis of phosphinyl, thiophosphinyl and phosphonio guanidines, *J. Organomet. Chem.* 529 (1997) 257–265.
- [33] F. Pazoki, F. Mohammadpanah, A.S. Manesh, J.A. Mehraban, A. Heydari, Diphenyl phosphate creatine immobilized on magnetite nanoparticles: an efficient and recyclable catalyst for Aza-Michael reaction, *J. Chem. Sci.* 132 (2020) 30.
- [34] K. Gholivand, A.A. Ebrahimi Valmoozi, M. Rahimzadeh Dashtaki, F. Mohammadpanah, M. Dusek, V. Eigner, M. Pooyan, M. Bonsaii, M. Sharifi, M. Ghadamyari, Synthesis, crystal structure, fluorescence assay, molecular docking and QSAR/QSPR studies of Temephos derivatives as human and insect cholinesterase inhibitors, *ChemistrySelect* 2 (2017) 8828–8840.
- [35] K. Gholivand, M. Pooyan, F. Mohammadpanah, F. Pirastefar, P.C. Junk, J. Wang, A.A.E. Valmoozi, A. Mani-Varnosfaderani, Synthesis, crystal structure and biological evaluation of new phosphoramidate derivatives as urease inhibitors using docking, QSAR and kinetic studies, *Bioorg. Chem.* 86 (2019) 482–493.
- [36] M. Alabboud, A. Javadmanesh, *In silico* study of various antiviral drugs, vitamins, and natural substances as potential binding compounds with SARS-CoV-2 main protease, *DYSONA Life Sci.* 1 (2020) 44–63.
- [37] S. Adem, V. Eypuglu, I. Sarfraz, A. Rasul, M. Ali, Identification of potent COVID-19 main protease (M^{pro}) inhibitors from natural polyphenols: an in silico strategy unveils a hope against CORONA, Preprints (2020) 2020030333.
- [38] W. Dai, B. Zhang, X.M. Jiang, H. Su, J. Li, Y. Zhao, X. Xie, Z. Jin, J. Peng, F. Liu, Structure-based design of antiviral drug candidates targeting the SARS-CoV-2 main protease, *Science* 368 (2020) 1331–1335.
- [39] P.W. Kenny, Hydrogen bonding, electrostatic potential, and molecular design, *J. Chem. Inf. Model.* 49 (2009) 1234–1244.
- [40] B. Kosar, C. Albayrak, Spectroscopic investigations and quantum chemical computational study of (E)-4-methoxy-2-[(p-tolylimino) methyl] phenol, *Spectrochim. Acta Part A Mol. Biomol. Spectrosc.* 78 (2011) 160–167.
- [41] D. Lewis, C. Ioannides, D. Parke, Interaction of a series of nitriles with the alcohol-inducible isoform of P450: computer analysis of structure-activity relationships, *Xenobiotica* 24 (1994) 401–408.
- [42] T. Lu, F. Chen, Multiwfn: a multifunctional wavefunction analyzer, *J. Comput. Chem.* 33 (2012) 580–592.
- [43] I. Fleming, *Frontier Orbitals and Organic Chemical Reactions*, Wiley, 1977.
- [44] T.E. Tallei, S.G. Tumilaar, N.J. Niode, B.J. Kepel, R. Idroes, Y. Effendi, S.A. Sakib, T.B. Emran, Potential of plant bioactive compounds as SARS-CoV-2 main protease (M^{pro}) and spike (S) glycoprotein inhibitors: a molecular docking study, *Scientifica* 2020 (2020) Cairo.
- [45] R. Parthasarathi, V. Subramanian, D.R. Roy, P. Chattaraj, Electrophilicity index as a possible descriptor of biological activity, *Bioorg. Med. Chem.* 12 (2004) 5533–5543.
- [46] R.G. Parr, L.V. Szentpály, S. Liu, Electrophilicity index, *J. Am. Chem. Soc.* 121 (1999) 1922–1924.
- [47] R.G. Parr, R.G. Pearson, Absolute hardness: companion parameter to absolute electronegativity, *J. Am. Chem. Soc.* 105 (1983) 7512–7516.
- [48] E.R. Johnson, S. Keinan, P. Mori-Sánchez, J. Contreras-García, A.J. Cohen, W. Yang, Revealing noncovalent interactions, *J. Am. Chem. Soc.* 132 (2010) 6498–6506.
- [49] W. Humphrey, A. Dalke, K. Schulten, VMD: visual molecular dynamics, *J. Mol. Graph.* 14 (1996) 33–38.
- [50] G. Saleh, C. Gatti, L.L. Presti, Non-covalent interaction via the reduced density gradient: independent atom model vs experimental multipolar electron densities, *Comput. Theor. Chem.* 998 (2012) 148–163.
- [51] A.E. Reed, L.A. Curtiss, F. Weinhold, Intermolecular interactions from a natural bond orbital, donor-acceptor viewpoint, *Chem. Rev.* 88 (1988) 899–926.
- [52] A.C. Wallace, R.A. Laskowski, J.M. Thornton, LIGPLOT: a program to generate schematic diagrams of protein-ligand interactions, *Protein Eng. Des. Sel.* 8 (1995) 127–134.
- [53] Dassault Systemes BIOVIA, Discovery Studio Modeling Environment, Dassault Systemes, San Diego, CA, 2015 Release 4.5.
- [54] R. Todeschini, V. Consonni, A. Mauri, M. Pavan, DRAGON-Software for the calculation of molecular descriptors. Version 4.0 for Windows (2004).
- [55] M. J. Frisch, et al., Gaussian 03, Revision B.04, Gaussian, Pittsburgh, PA, 2003.
- [56] A.M. Petrescu, M.V. Putz, G. Iliu, Quantitative structure-activity/ecotoxicity relationships (QSAR/QEcoSAR) of a series of phosphonates, *Environ. Toxicol. Pharmacol.* 40 (2015) 800–824.
- [57] L. Wang, A hybrid genetic algorithm-neural network strategy for simulation optimization, *Appl. Math. Comput.* 170 (2005) 1329–1343.